Synthetic Separation Control Using Vortex Generator and Slot Jet in a High Load Compressor Cascade

J. Hu[1†], R. Wang[1], P. Wu[1] and F. Li[2]

[1] *School of Aeronautics and Astronautics Engineering, Air Force Engineering University, Shaanxi Xi'an 710038, China*
[2] *Chongqing University of Science and Technology, Chongqing 401331, China*

†*Corresponding Author Email: tryme@buaa.edu.cn*

ABSTRACT

The compressor cascade performance is significantly restricted by the secondary flow mainly presented as the trailing edge separation and corner stall. This paper develops a synthetic flow control approach in a high turning cascade using the vortex generator and slot jet approach. Numerical simulations were conducted to assess the flow control benefits and illustrate the flow control mechanisms. Four configurations, the baseline, the two individual approaches and the synthetic approach, were simulated to compare the separation control effects. The simulations show that all the three configurations achieve considerable improvements of the cascade performance and the cascade sensitivity to incidence angle is greatly decreased. The synthetic approach improves the most among them which is almost the superposition of the two individual ones. In the synthetic approach, the trailing vortex induced by the vortex generator suppresses the end wall cross flow and deflects the passage vortex, and then prevents the production of corner stall; at the same time, the slot jet speeds up the trailing edge separation caused by the cascade high camber. Owing to the combination of the two aspects, the synthetic approach restricts the developments of secondary flow and vortices in the cascade, and improves the outflow uniformity. The synthetic approach nicely utilizes the advantages of the two individual approach while avoids the shortages by the complementation, so it can achieve more powerful flow control effects. At the end, vortices models are established to illustrate the secondary flow structure and the flow control mechanisms.

Keywords: Compressor cascade; Flow control; High load; Vortex generator; Slot jet; Synthetic separation control.

NOMENCLATURE

C	chord	S_V	separation vortex
C_p	static pressure rise coefficient	*Slotted*	slotted blade
CS_V	Concentrated Shedding Vortex	SW_V	Span Wise vortex
C_V	corner vortex	TE	Trailing Edge
H_V	horseshoe vortex	TS_V	Trailing edge span wise vortex
i	incidence angle	VG	Vortex Generator
LE	Leading Edge	VG_V	VG trailing vortex
MS	Middle Span		
M_{is}	Isentropic Mach number	ω	total pressure loss coefficient
P	static pressure	$\Delta\beta$	flow turning angle
P_0	total pressure	δ	thickness of inlet boundary layer
P_{in}	inlet pressure	β_{1k}	inflow angle
P_V	passage vortex	β_{2k}	outflow angle

1. INTRODUCTION

The high load compressor trends to be the key part of aero-engine for the next generation as it contributes to fewer weight and fuel consumption. However, high load design always causes more complex secondary flow (Gbadebo *et al.* 2005), and increases the cascade sensitivity to the incidence angle (Liu *et al.* 2016). Separation suppression and flow stability enhancement for the high load compressor blade become an urgent issue in turbomachinery society.

At present, several active and passive flow control applications have been developed in linear cascade. The applications can be classified into two types based on the energy source. The first type is actuator, such as jets (Hecklau *et al.* 2011), plasma actuation (Akcayoz *et al.* 2015), and suction (Guo *et al.* 2013), *et al.* Actuators always need external input devices and additional energy consumption. The second type is geometric shape, such as end-wall contouring (Varpe *et al.* 2015), end-wall fences (Govardhan *et al.* 2012), vortex generator (Pesteil *et al.* 2010; Hergt *et al.* 2006, 2013; Wu *et al.* 2016), slot jet (Wu *et al.* 2013, 2014; Hu *et al.* 2016, 2017), *et al.* Geometric shape usually operates by some geometric design which induces some special flow behaviors and improve the flow field. The geometric shape applications usually need no additional input devices. On the other hand, it is now feasible to design and manufacture tiny features on the compressor surface. So it is now feasible to use the geometric shape application in the compressor cascade. The vortex generator and slot jet approach exhibit considerable prospect among the presented technologies because they need no extra input device.

Vortex generator (VG) is initially designed as a mini vane, which creates an exogenous vortex and counter balancing the endogenous vortex. The vortex generator is able to re-energize the low momentum boundary layer and delay the separation. Hergt *et al.* (2006, 2013) conducted a series of studies on three types of vortex generator configurations. They reported that different types and placements of vortex generator applications all achieved a significant reduction of cascade loss and load at the cascade mid-span, which led to a shifting of the operating range or rather the stall boundary towards higher positive incidence angles. Presteil at al. (2010) introduced the vortex generator to the compressor "CREATE". The results showed that VGs enabled to reduce the flow loss and improve the stability in high load devices due to better flow turning effects near the casing. Wu *et al.* (2016) illustrated the flow control mechanisms of the vertex generator in a high load cascade using a 3D geometric model. The vortex generator was verified to be effective in the cascade.

A slot jet approach was developed to reduce the separation in compressor blade by Ramzi (2013), Wu *et al.* (2013, 2014) and Hu *et al.* (2016, 2017). A slot which connected the flow field between pressure side and suction side was inserted into the blade. Because of the pressure difference, the slot produced self-induced jet from the pressure side to the suction side. The parameters studies in terms of the slot location, the slot shape, and the jet angle were numerically investigated. Experiment measurements proved that the jet flow was very effective in mixing and energizing the suction side separation. As the cascade separation was delayed, the cascade performance achieved considerable improvements.

The previous studies show that the VG operates by suppressing the end wall crossflow then delaying the corner stall. The slot operates by the jet flow which enables to suppress the cascade separation (Hu *et al.* 2016, 2017) caused by the high camber. The ways of separation reduction of the two individual approaches show a considerable prospect in combination usage. On the other hand, the high load cascade requires more **powerful flow** control applications. Therefore, this paper develops a synthetic approach using the VG and slot, expecting for more powerful effects. The main objects focus on the optimizing design of combining the advantages of VG and slot while avoiding the shortages. Numerical study will be performed to assess the effect and explore the flow control mechanisms in details.

2. CASE DESIGN

The baseline configuration is a high load compressor cascade. The profile is the section at 10% of span distance from the hub of the last row stator vanes of the axial, 2.5-stage, high load transonic compressor. The inlet operating velocity of the cascade is 0.6 *Ma* (Mach number). The detailed information of general design parameters are listed in Table 1. The baseline cascade is a typical high turning diffuser with camber angle 62.81° and diffusion factor 0.52. So it is very sensitive to incidence angle at off-design conditions. Large scale trailing edge separation and corner stall will emerge at the large incidence angle. Therefore, it is appropriate for checking the actual ability of the synthetic flow control approach.

**Table 1 Design parameters of the baseline cascade**

Parameters/unit	Value
Chord length(C)/ mm	60.7
Solidity($\tau = C/S$)	2.55
Aspect ratio($AR=L/C$)	1.65
Inlet angle(β_{1k}) / (°)	33.46
Outlet angle(β_{2k}) / (°)	96.27
Stagger angle(γ)/ (°)	25.01
Turning angle(θ)/(°)	62.81
Diffusion factor (-)	0.52

For the VG configuration, the design parameters have been carefully selected and proved to be effective in the previous studies by Wu *et al.* (2016). So these

parameters will continue to be used in this study as presented in Fig.1 (a). The vortex generator is a small vane linearly stacked by NACA64-006 airfoil. The VG height is $4/3\delta$. The VG chord length is 13%C. The VG chord line has 16° skewing with the cascade chord line.
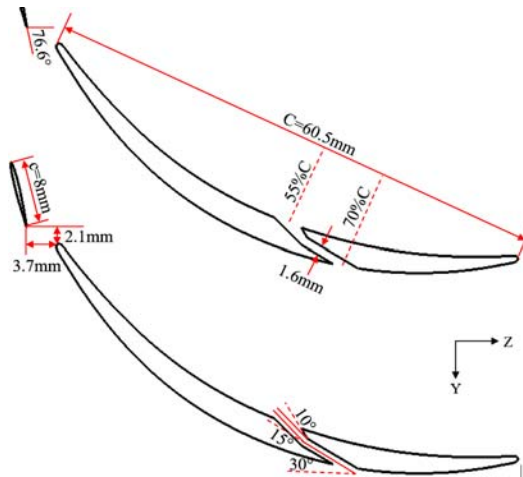
(a) Design parameters
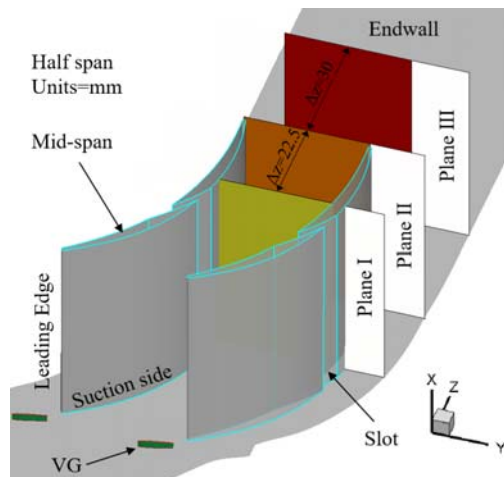
(b) Three-dimensional model

Fig. 1. Design parameters and geometric models.

For the slot configuration, the parameters are also selected by a series of parameters studies by Wu *et al.* (2013, 2014) and they will continue to be use here. The slot profile is presented in Fig.1 (a). A two-part slot is designed that the first part (inlet part) is a convergence channel by 10° which enables to accelerate the jet flow, and the second part (outlet part) is a parallel channel acting as ejector. In order to improve the inlet pressure of the jet flow, the slot inlet part turns to the downstream by 15°. Inlet and outlet position of the slot are respectively 55%C and 70%C.

For the synthetic configuration, the geometric arrangement is a direct addition of the two individual approach. The arrangement is displayed in Fig.1 (a). Three-dimensional model of the synthetic configura-

tion is displayed in Fig.1 (b).

3. NUMERICAL SCHEME

3.1 Simulation Method

Single-passage simulations are performed in the CFX solver to solve three-dimensional steady Reynolds-Averaged Navier-Stokes equations. Second-order upwind, implicit, and time-marching scheme are used. Energy equation and compressible model are also solved. SST k-omega turbulence model is used to enclose the discrete equations. A transition model is applied to capture the transient features. The convergence criterion is 1×10^{-6} in magnitude, at the same time the mass flow deviation between inlet and outlet should be smaller than 0.1%.
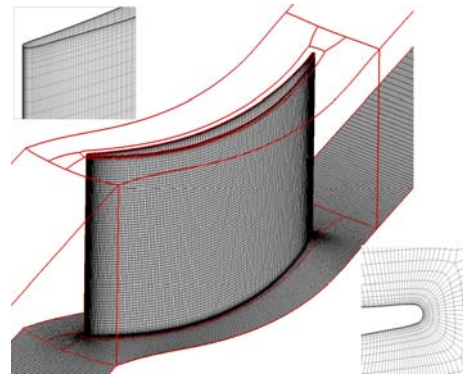
(a) Grid topology and wall grid
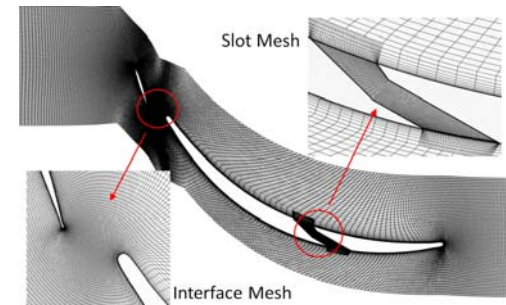
(b) Grid detailed for connections and small characteristic

Fig. 2. Schematic map for calculated grids.

Figure 2 (a) displays the grid topology and wall grid in the baseline cascade. The cascade is covered by O-block while the other parts are filled with H/I-blocks. The grids are automatically generated in AutoGrid5 software. When generating the grid for VG case, the flow field is divided into two rows, namely VG row and main blade row. None interface is used between two rows to ensure the grid nodes of the two sides are one-to-one correspondence. This technic fully eliminates the numerical errors caused by interfaces, which is fatal for predicting the teeny localized VG wake. For the slot case, an additional block is inserted to the generated grids using IGG tool. The initial grid out
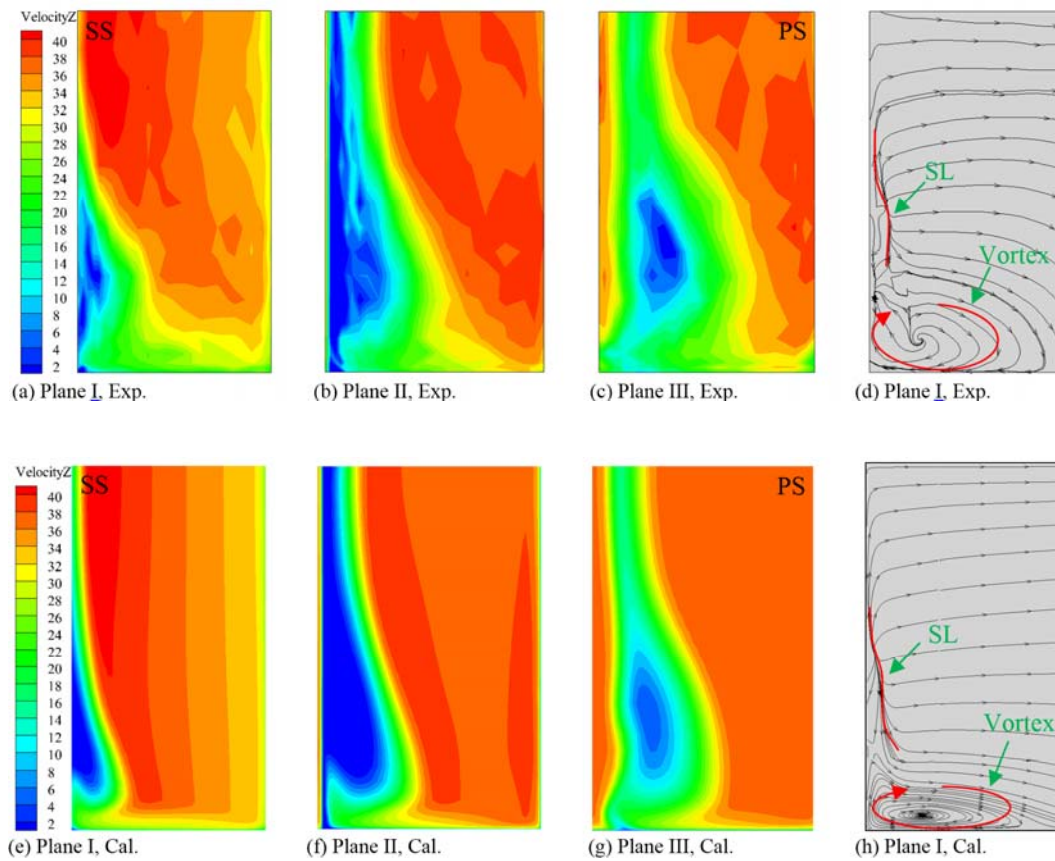
Fig. 3. Velocity distributions on cascade z-axis planes (S3) of experiment (up) and calculation (down).

side of the slot remains the same, only the density of the grid adjacent to slot inlet and outlet are increased. VG and main blade are covered by O block as the boundary layer grid. Periodic interfaces between single passage sides are also one-to-one correspondence.

All the first layer cells near wall are clustered by 1.67μm to ensure y+=1. The grids in the slot and around VG are densely clustered to capture the small flow structure. Detailed grids of the interface and the slot are shown in Fig.2 (b). The number of grid nodes in cascade passage is 3187723. The grid independence is checked before the simulations. The number of grid nodes in the slot is 243309.

At the cascade inlet, the inflow velocity is assigned to 0.6 Ma by defining the velocity components at different incidence angles. The total temperature is 288.15K. The inflow boundary layer is defined as the velocity deficit and the thickness (δ) is based on the value reported by Chima (2002). At the cascade outlet, averaged static pressure over the pitch is given. The other flow parameters are extrapolated by the calculations. Blade surface and sidewall are adiabatic and no slip wall. The working fluid is the ideal gas. The flow turbulence intensity is 1%. Reynolds number is about 8.74×10^5 based on inlet velocity and blade chord length.

3.2   Validations

To validate the numerical approach in this study, experiment measurement is applied to check the predictions in the baseline configurations. The experiment facility and procedure have been reported in details by Hu *et al.* (2017). The design operating condition is selected here as the validation datum, in which condition the three-dimensional flow field structure has been measured in details. The contours as well as the streamlines on certain planes are compared for checking the prediction ability of separation behaviors and the flow structure.

In the experiments, three axial (z-axis) planes are measured to show the 2D flow field as shown in Figure 1 (b). The first plane (Plane I) is located at the upstream of trailing edge by 22.5mm. The second plane (Plane II) is located at downstream of trailing edge by 1mm. The third plane (Plane III) is located

at the downstream of Plane II by 30mm. The contours of velocity z-axis component from measurements and simulations are presented in Fig.3.

According to the contours, it can be seen that the numerical predictions successfully predict the corner separation evolutions process. In the blade passage (Plane I), the separation cell only emerges at the low span. At the blade outlet (Plane II), the separation is

consisted of two parts, the corner stall cell caused by the end wall cross flow (Liu *et al.* 2016) and the trailing edge separation caused by the cascade camber. At the blade downstream (Plane III), the separation cell diffuses and bends. The simulations predict the major characteristics of the measurements nicely in terms of the separation locations, the low speed area, and the shape of separation zone, although the predicted separation is slightly smaller. Especially on the plane III, the predicted result agree very well with the experiments in terms of the boundary bend. In summary, the simulations predict the main features of the measurements.

In this study, the flow structure is the other focus that is used to illustrate the flow control mechanism. Therefore, the second validation is conducted on the Plane I concerning the 2D streamlines. In Fig.3 (d) and (h), the predicted passage vortex distribution and the separation line agree well with the measurement though the size of predicted vortex is smaller. It indicates that the simulations enable to predict the flow structure qualitatively. In conclusion, the numerical approach used in this paper is sufficient to predict this high load cascade flow.
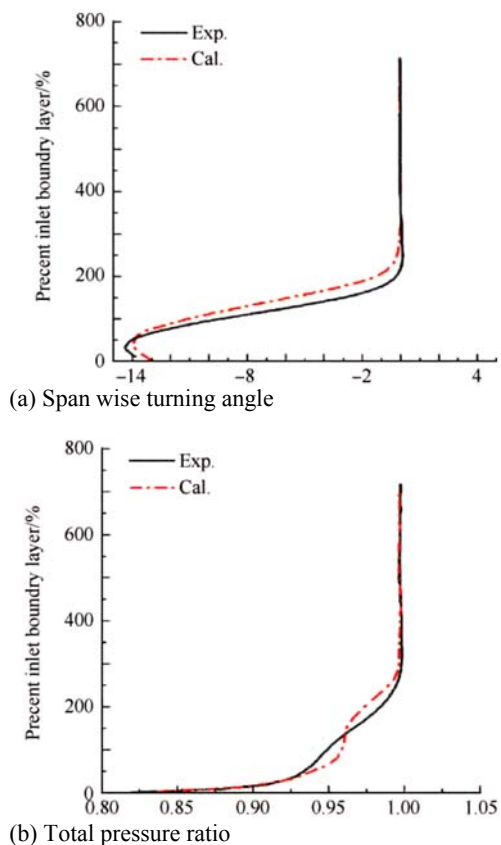

(a) Span wise turning angle

(b) Total pressure ratio

Fig. 4. Measured and predicted flow parameters of VG wake.

On the other hand, as the VG is a very tiny feature that only has height of $4/3\delta$, it is fatal for this tiny wake flow prediction. An additional validation is performed here to check the VG wake which only has the isolated VG. The measured results for the computational model are initially published by Chima (2002). The predicted results are compared with measurements as shown in Fig.4. The simulation predicts the span wise turning angle and the total pressure ratio nicely with the measurements, as it captures the value and trend of the two parameters along the span wise.

From the three parts of validations, it can be concluded that the numerical approach is accurate and sufficient enough for the present investigations.

4. CASCADE FLOW BEHAVIORS

4.1 Separation Behaviors

The secondary flow mechanisms in the baseline cascade and the improved cascade are numerically investigated in details to assess the flow control effects. Fig. 5 shows the Mach number contours on five typical sections (S1) along the span wise for the baseline and the synthetic configuration. The figures display the blade separation changes at two incidence angle. At incidence angle 0°, the baseline cascade separation is relatively small, and the largest separation is located on 15%span. The synthetic approach nicely delays the trailing edge separation and the corner stall cell. At incidence angle 3°, the separation of baseline cascade emerges a rapid increase in size and intensity. The blade corner is stalled by the large volume low momentum fluids. The rapid increase suggests that the cascade is extremely sensitive to the incidence angle and it is narrow in terms of the operating range.

In the synthetic configuration, the separated flow is well suppressed within all the span range. The trailing edge separation caused by the cascade camber is completely eliminated while the corner stall caused by the end wall secondary flow is significantly reduced. Comparing the flow fields at incidence angle 0° and 3°, the separation behaviors maintain the same level that the separation area does not increase although the incidence angle increases. It indicates that the synthetic configuration enlarges the stable operating range of the high camber cascade by reducing the separation.

Figure 6 shows the suction surface Mach number of at four configurations. The legend is same with Fig.5. Compared with the baseline cascade, the VG delays the separation start point and reduces the corner stall, but slightly increases the trailing edge separation. The slot almost eliminates all the trailing edge separation, but the corner stall before the slot outlet remains the same. The reason is that the jet flow induced by the slot cannot affect the separation before the slot outlet. In summary, the two individual approaches operate in different ways. The slot eliminates the trailing edge separation caused by the cascade camber while the VG reduces the corner stall caused by the end wall secondary flow. Naturedly, the two approaches present a nice prospect in combination usage.
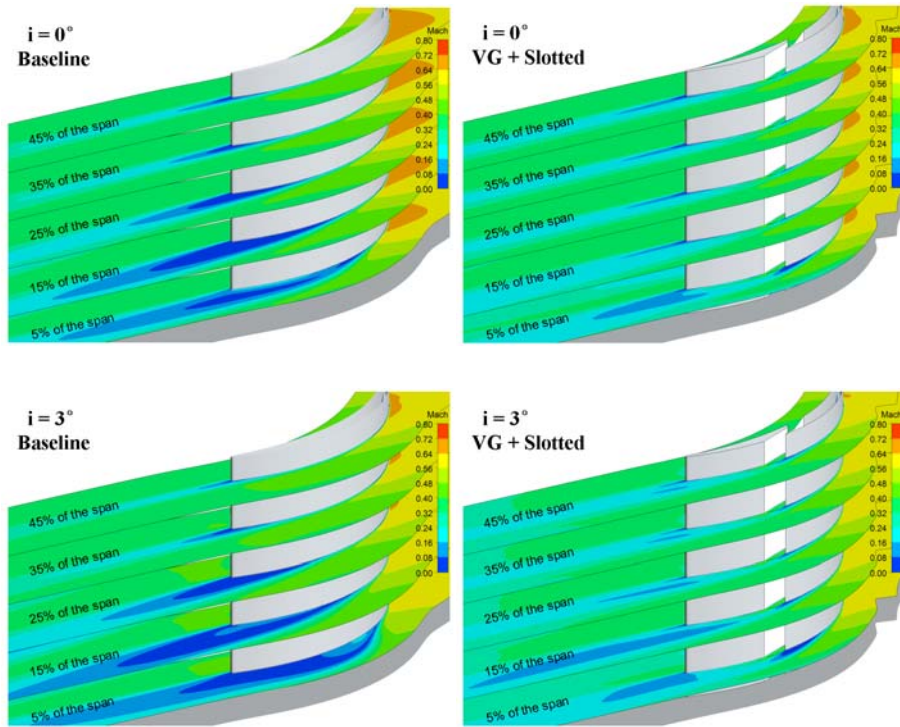
Fig. 5. Mach number contours on S1 flow surface.
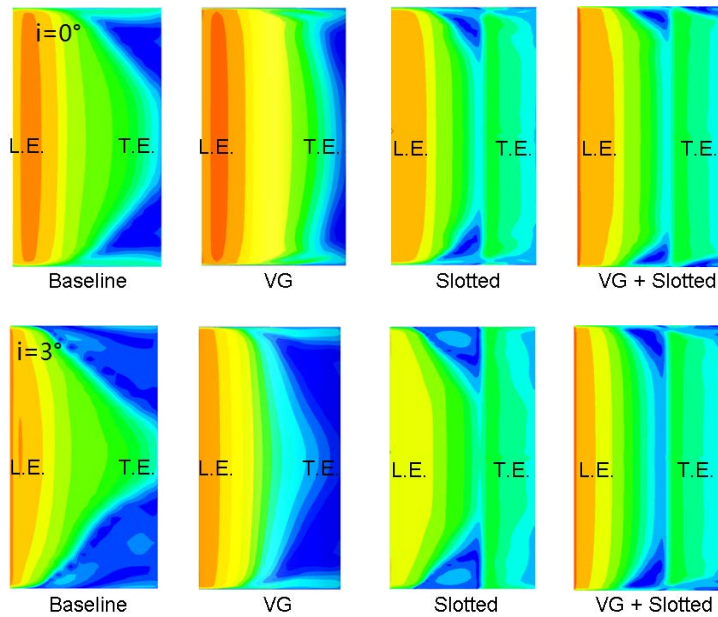

Fig. 6. Suction surface Mach number at four configurations.

So in the synthetic configuration, the flow control approach acquires better benefits than the two individual devices by combining their advantages that the slot eliminates the trailing edge separation while the VG reduces the corner separation before the slot outlet. The VG operates at the front of passage and slot operates at the back of passage at the same time. This cooperation is more close-knit when the incidence angle increases from 0° to 3°. In incidence angle 3°, the separation area is too large to be nicely reduced by the individual device, but the synthetic configuration exhibits powerful effectiveness on the huge separation condition.
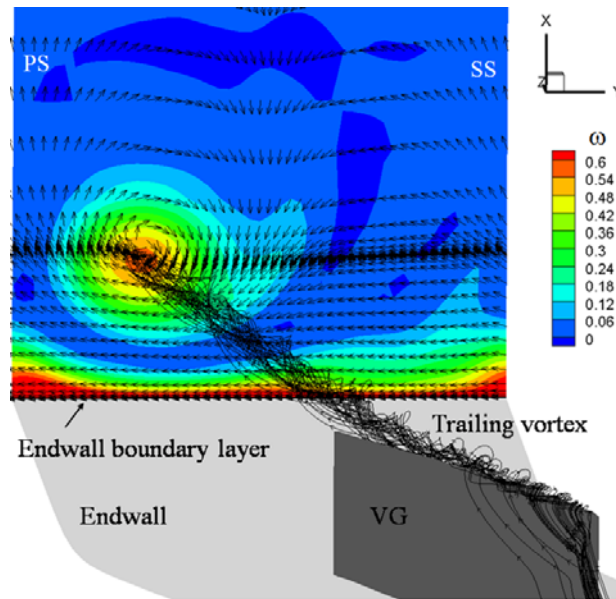
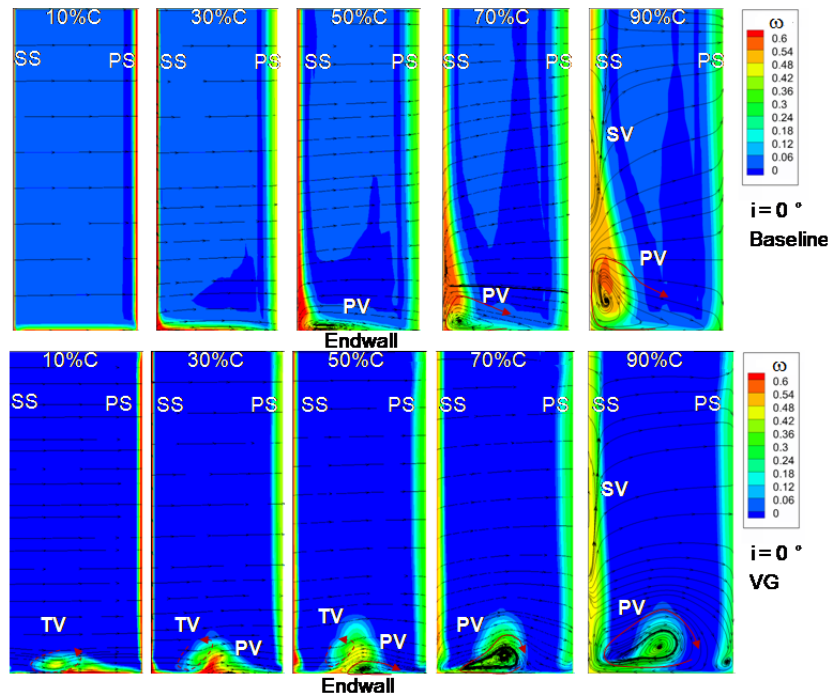**Fig. 7. VG trailing vortex and its flow loss characteristic.**

Fig. 8. Evolution process of VG trailing vortex (TV) and passage vortex (PV).

4.2 Influence of VG and Slot

To illustrate the operating mechanism of the synthetic configuration, the two individual devices will be discussed respectively in this section. Fig. 7 presents the wake vortex induced by the VG. Downstream the VG by double VG axial chord length, an additional plane is displayed to show the total pressure loss efficiency (ω) and the 2D vectors.

The inflow cross over the VG and produces a vortex which rotates in the clockwise. The vortex produces extra flow loss and the peak loss corresponds to the

vortex core. In the baseline cascade, the vectors in the boundary layer march on the end wall from pressure side to suction side due to the pressure gradient. However, the boundary layer vectors under the VG vortex are forced to change the direction, from pressure side to suction side, as the VG wake vortex rotates in this direction. This phenomenon will be further analyzed later.

Figure 8 presents the vortex evolution process in the baseline and the VG configuration at the design point. The planes are located at the blade passage with

different chord length (C). The figure shows that the VG wake vortex rotates in the counter direction with the blade passage vortex. The trailing vortex changes the flow structure of the baseline cascade by interacting with the passage vortex.

In the baseline cascade, the passage vortex onset is approximately located at 30%C and finally shapes up at 70%C. At the 90%C, the passage vortex merges with the trailing edge separation and then becomes a large scale vortex that locates at the blade corner. The formation process of the corner separation indicates that the passage vortex is potentially responsible for the corner stall, so the suppression of passage vortex may reduce the corner stall. The corner separation investigations also reported that the passage vortex may catalyze the formation of corner stall by Liu *et al.* (2016).

In the VG configuration, the VG wake vortex has shaped up at the 10%C. The vortex gradually changes the boundary layer shape and thickness. At the 30%C, the passage vortex begins to emerge and interact with the VG vortex due to their counter rotating direction. The boundary layer between the suction surface (SS) and the VG vortex is eliminated as the boundary layer fluids is pushed towards the pressure surface. At the 50%C, the VG vortex meets the passage vortex and forms a high loss area at passage middle. Compared with the baseline, the passage vortex is obviously pushed awards the pressure surface and it is insulated with the corner separation. The passage vortex in the VG case locates at the middle of the blade passage all the time while accumulates to the blade corner in the baseline, and its size is also reduced. At the 90%C, the VG vortex gradually dissipates but the passage vortex always stays at the passage middle. As a result, the formation of the general corner stall is delayed and weakened.

In conclusion, the VG operates by producing a wake vortex, which rotates in the counter direction of passage vortex. The VG vortex delays the formation of passage vortex and pushes it towards the passage middle. In this way, the VG prevents the passage vortex from forming the general corner stall.

On the other hand, the operating mechanism reversely indicates that the VG is unable to influence the high span range separation caused by the cascade camber. So the extra slot jet approach is necessary for this high camber cascade.

Figure 9 chooses the flow field of the largest separation span to illustrate the operating mechanisms of the slot jet approach. The figures present the axial velocity and 2D streamlines at the span of 15% and at incidence angle 3°.

In the baseline cascade, the large separation zone emerges at the suction side trailing edge which is filled with two counter rotating vortices. The cascade flow is severely stalled by the separation zone that the area of equivalent outlet and the flow turning angle are decreased to some extent.
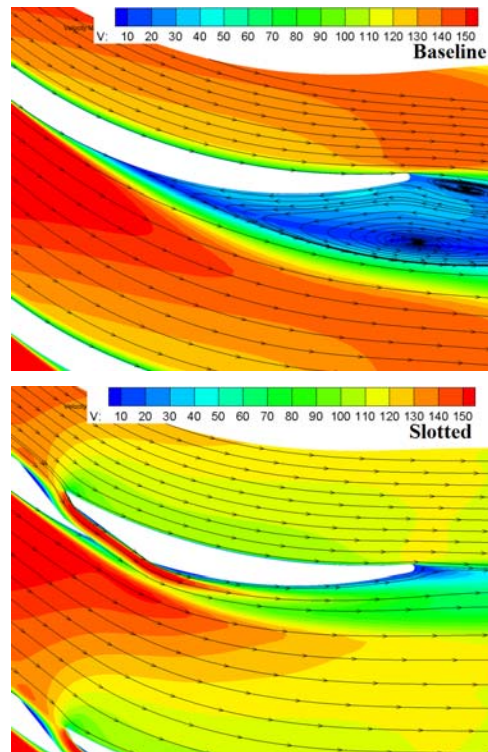

Fig. 9. Velocity magnitude and streamlines on 15% span at *i*=3°.

In the slot configuration, the slot induces a branch of high speed jet flow to the suction side. The jet flow is initially designed to inject into the separation area, which is used to improve the momentum of the separated fluids and prevent them from accumulation. The result verifies the design purpose that the separation is completely blown away by the jet flow and the streamlines reattach to the suction surface. The speed in the initially separated location is still slower than the main flow, but the backflow and vortices are completely eliminated.

Once the separated streamlines reattach to the suction surface, the area of equivalent outlet increases about 25% at the cascade outlet. It is noticeable that the main flow which initially outside the separation zone is decelerated at the cascade outlet. The reason is that in a subsonic diffuser the fluids will decelerate and elevate the pressure, and the decelerating ratio positively corresponds to the ratio of equivalent outlet area to inlet area. In the cascade, the ratio improvement will contribute to a lower outlet speed, higher flow turning angle and higher static pressure rise.

Figure 10 presents the distribution of static pressure rise coefficient (C_p) corresponding to Fig.9. The figure verifies the pressure difference between the slot inlet and outlet which drives the jet. In the slot cascade, static pressure rise is considerably improved at both the pressure and suction side. The overall static pressure rise coefficient is significantly improved at the cascade outlet. The reason is the increase of the equivalent outlet area as illustrated.
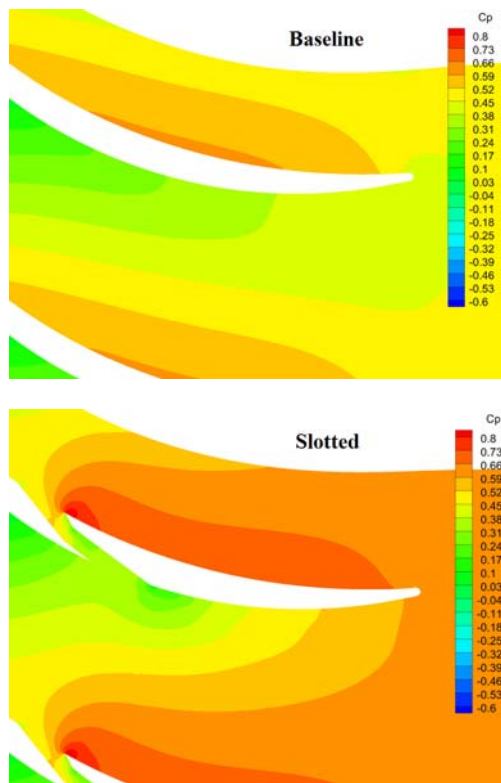
Fig. 10. Static pressure rise coefficient on 15% span at *i*=3°.

On the other hand, the airflow leakage from pressure side to suction side will decrease the cascade aerodynamic load. Fortunately, the improvement of equivalent outlet area bridges the gap and further increase the cascade aerodynamic load.

5. CASCADE PERFORMANCE

The impacts of separation control devices presented above indicate a good prospect of improving the characteristic of the cascade. Fig. 11 and 12 respectively show the modified loss characteristic and the cascade performance lines at four configurations.

Fig.11 presents the loss distribution on the cascade outlet plane at incidence angle 0° and 3°. In the baseline cascade, the loss is caused by the trailing edge separation and corner stall. The two sources of separation merge together and form a large separation area. In the VG configuration, the VG vortex prevents the passage vortex from merging with the trailing edge separation as illustrated in Fig.8. So the loss is separated into two parts, the trailing edge separation loss on the suction surface, and the passage vortex loss at the passage middle. The total loss decrease significantly mainly because the reduction of the corner stall. In the slot configuration, the jet flow accelerates the low speed fluids within all the span, so the loss is reduced at all the span. The slot reduces the loss intensity but the loss area remains the same. In the synthetic configuration, the two individual approaches operate at the same time. The slot reduces the loss intensity at all the span while the VG vortex delays the for-

mation of corner stall and reduces the end wall flow loss. As a result, the synthetic approach achieves better separation effects than the individual two.

Compared with the incidence angle 0°, the synthetic approach is more sufficient and effective at the larger separation condition of incidence angle 3°, indicating that the combination usage is more effective at the large separation condition. The loss barely grows from incidence angle 0° to 3° in the synthetic configuration, indicating the cascade operating range is enlarged at least 3° in terms of the incidence angle.

Figure 12 presents the cascade performance at four configurations. Compared with the baseline, the VG configuration reduces the total pressure loss (ω) and increases static pressure rise (C_p) within all the operating conditions, but the flow turning angle ($\Delta\beta$) remains the same with the baseline. In the slot cascade, the three performance parameters achieve considerable improvements at the incidence angle from 0° to 4°. At incidence angle -1°, the slot has little impact on the cascade performance. But when the incidence angle is smaller than -1°, the slot induces negative impacts. The reason is that the slot outlet locates before the separation points under this condition, so the jet flow directly injects into the main flow which causes extra loss and negative impacts (Hu *et al.* 2016).

In sum, the two individual approaches are effective to improve the cascade performance, but both the two have some shortcomings. The VG is inefficient for improving the flow turning angle, and the slot is negative when the incidence angle is smaller than -1°.

In the synthetic configuration, the cascade performance achieves significant improvement in all the operating conditions. When incidence angle is larger than -2°, the cascade performance is the superposition of the two individual ones. At incidence angle -2° to -4°, the negative impacts of the slot is eliminated by the VG. The inefficient of VG in terms of the flow turning angle is also improved by the slot. The combination shows its high efficiency by combines the advantages while avoiding the shortages of the two individual ones.

In summary, the synthetic approach is more powerful with no negative impact in all the operating conditions. Comparing the loss characteristic lines, the line's slope of the synthetic configuration is the smallest, indicating that the cascade sensitivity to incidence angle is greatly decreased. The operating stability of the high load cascade acquires considerable improvements.

Table 2 shows the performance improvements of the four configurations averaged from all the incidence angles. Compared with the baseline, the VG works better on reducing the loss and increasing the static pressure rise, while the slot works better on increasing the flow turning angle. The synthetic approach acquires the largest improvements in which the performance parameters are almost the superposition of the two individual ones.
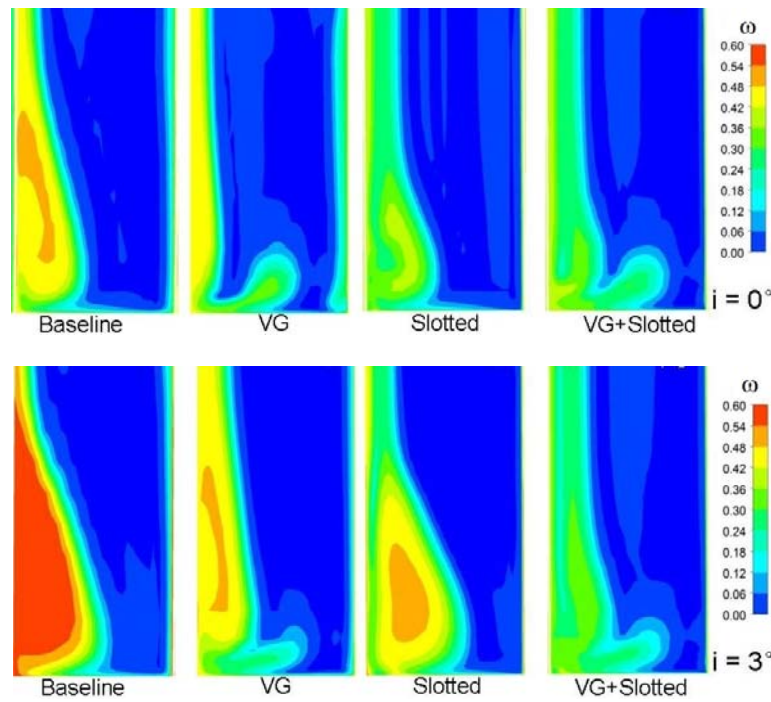
Fig. 11. The loss characteristic at blade outlet at four configurations.

Tab 2 Averaged performance gain compared to the baseline

Parameters	$-\omega$ (%)	C_p (%)	$\Delta\beta$ (%)
Slotted	2.92	1.46	0.95
VG	11.03	4.05	0.09
VG+ Slotted	13.75	4.88	1.91

6   FLOW CONTROL MECHANISMS

6.1 Boundary Layer Flow

The boundary layer flow pattern always reflects the secondary flow and separation behaviors in the cascade flow. Fig. 13 shows the limiting streamlines on the end wall. In the baseline cascade, the inflow boundary layer accumulates from the pressure surface toward the suction surface as the red arrows show. This phenomenon is generally called the end wall cross flow. The cross flow forms a span wise vortex locating at about 30% chord length near the suction surface. A separation line, which indicates the boundary of the corner vortex, locates downstream the span wise vortex. The corner vortex develops along the adverse direction of the main flow between separation line and suction surface. Vortex recognition in this paper refers to the vortices model reported by Kang (1993).

In the VG configuration, a convergence line replaces the initial vortex core on the end wall. The inflow boundary layer is divided into two parts by the con-

vergence line. The first part is between the suction surface and convergence line, and the second part is between the convergence line and pressure surface. Astride the convergence line, the boundary layer march forward the adverse direction as the red arrows showing. The first part reverses its initial flow direction as described in Fig.7. Therefore, part of the general cross flow in the cascade is eliminated, and then the separation start point is delayed. The start point of the separation line moves from about 40%C to 60%C downstream. The span wise vortex is totally eliminated in this configuration.

In the slot configuration, the cross flow before the slot stays the same. The cross flow pattern, the span wise vortex and the separation line are quite similar with the baseline cascade. But at the slot inlet, the streamlines are suctioned into the slot, and at slot outlet the streamlines are pushed away from suction surface. A convergence line replaces the separation line at the blade corner, indicating that the corner vortex is eliminated by the jet flow. The separation line behind the slot outlet is pushed toward the passage middle. Suction at slot inlet and jet at outlet, the slot also reduces the end wall cross flow.

In the synthetic configuration, two devices take part in the flow control. In the front of the cascade passage, the VG eliminates the span wise vortex by delaying part of the cross flow. In the back of the cascade passage, suction at slot inlet and jet at slot outlet reduce the cross flow development and eliminate the corner vortex. As a result, the cascade end wall cross flow is

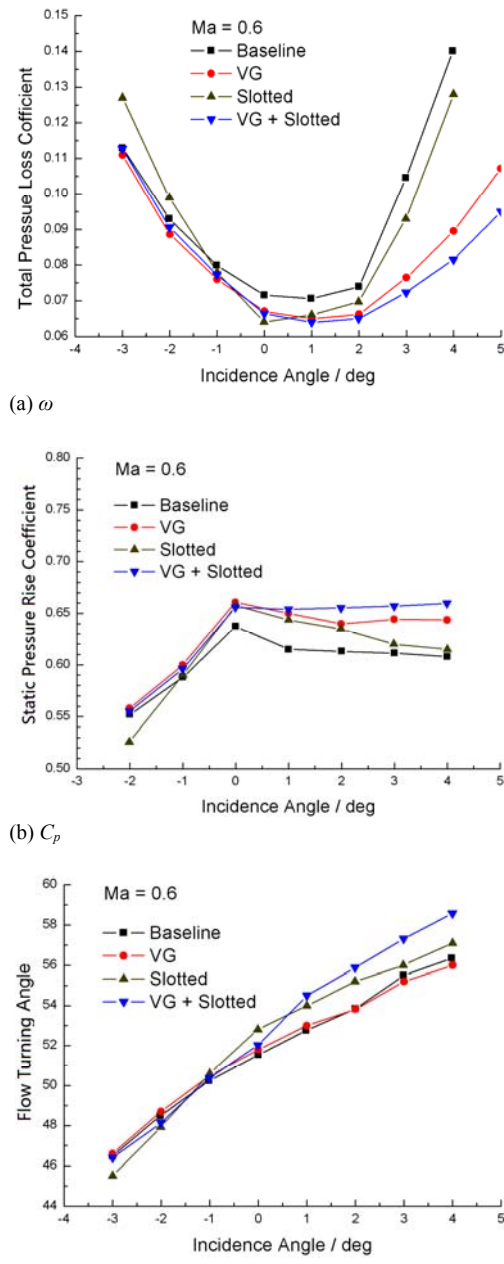nicely suppressed by the combination usage.

(a) ω

(b) C_p

(c) $\Delta\beta$

Fig. 12. Cascade performance at four configurations.

Figure 14 shows the limiting streamlines on suction surface. In the baseline cascade, the separation behaviors are presented by the boundary layer flow pattern. The VG delays the start point of separation, so the corner separation is reduced in size. It is noted that a slight increase of separation emerges at the middle span. In the slot cascade, the separation pattern before the slot outlet stays similar with the baseline, including the backflow and its span wise ascent. Behind the slot outlet, the backflow is clearly eliminated. In the synthetic configuration, the start point of separation is delayed and the backflow before slot outlet is limited

to corner by the VG. The back flow behind slot outlet is eliminated and reattaches to suction surface by the slot. It can be concluded that the synthetic approach achieves the best flow control effects by the synthetic effects of the two individual approaches, and the outlet flow is clearer with fewer secondary flow and vortices.
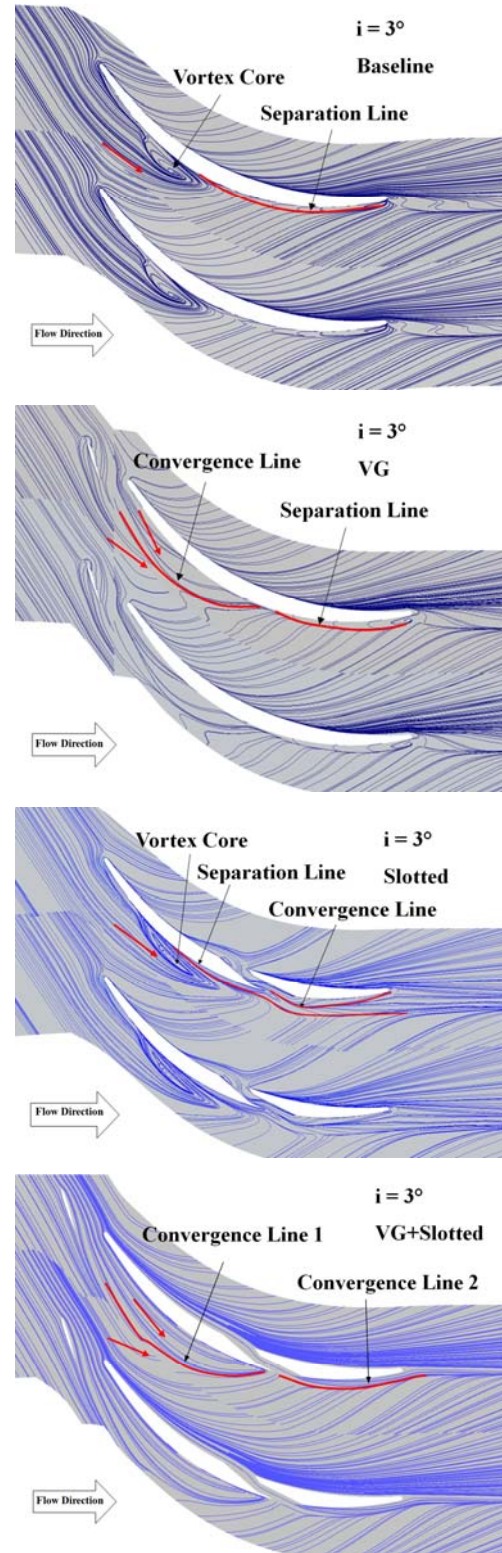

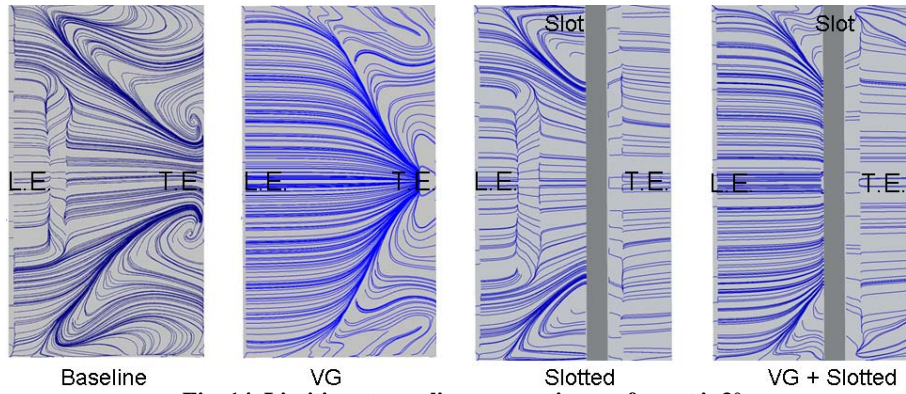**Fig. 13. Limiting streamlines on side wall.**

Fig. 14. Limiting streamlines on suction surface at i=3°.

(a) Baseline

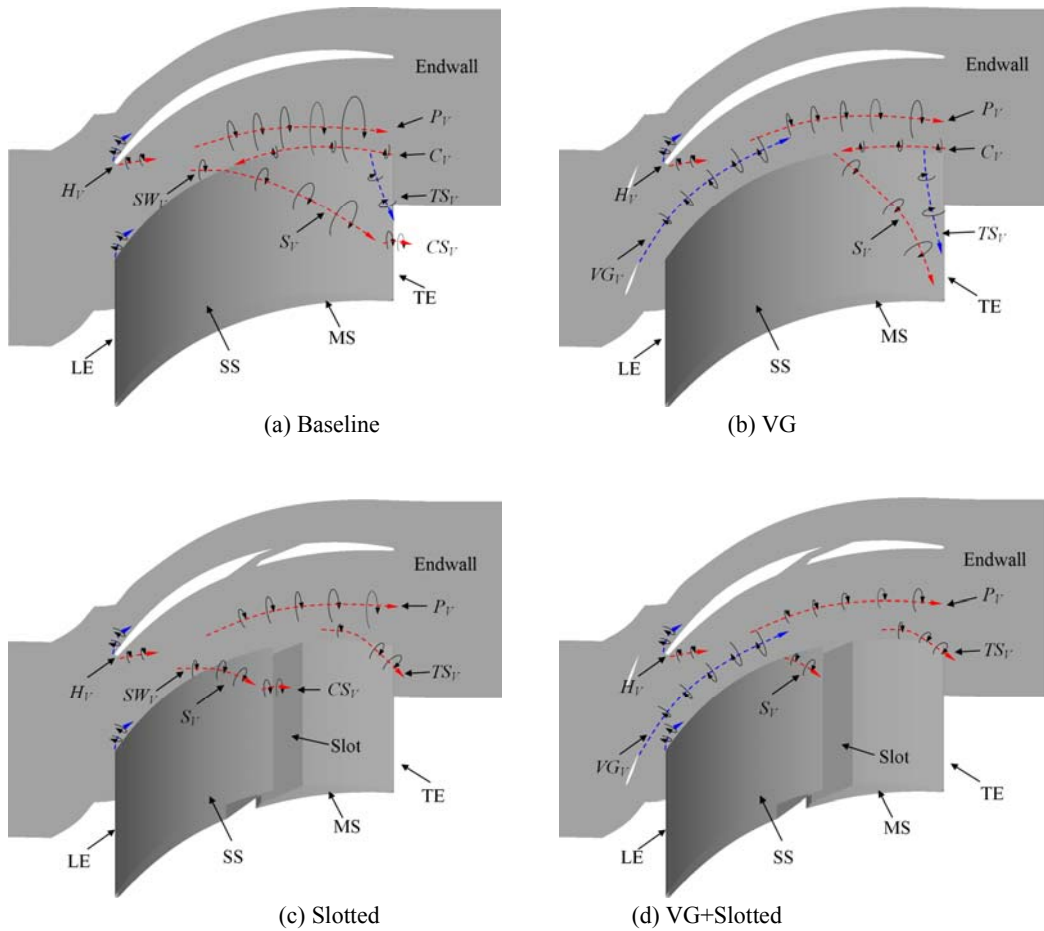(b) VG

(c) Slotted

(d) VG+Slotted

Fig. 15. Vortices models for four configurations.

6.2 Vortices Structure

Simplified vortices model is established in this section to illustrate the flow control mechanisms in different configurations. To underline the key point, small vortices are ignored. The establishing process of the vortices model are simplified based on the analysis above. The main vortices are presented in the models, such as the trailing edge span wise vortex (TS_V), the concentrated shedding vortex (CS_V), the separation vortex

(S_V), the horseshoe vortex (H_V), the passage vortex (P_V), the VG wake vortex (VG_V), the span wise vortex (SW_V), and the corner vortex (C_V). Blue lines represent the clock-wise rotation while red lines represent the counter direction.

Comparing with the baseline in Fig15 (a), VG adds an extra vortex of the VG_V to cascade passage (Fig15 (b)). The vortex rotates with a counter direction of the passage vortex, so the size of the passage vortex is

reduced due to the interaction. The VG vortex also prevents the passage vortex from merging with the corner separation, and the passage vortex is pushed to the passage middle. The VG vortex reverses part of the end wall cross flow and delays the separation start point, so the separation vortex and the trailing edge span wise vortex are minified. But both the two vortices extend to 50% span and induces slight negative effects at about 45%-50% span range. The span wise vortex and the concentrated shedding vortex are eliminated completely by the VG.

In the slot cascade (Fig.15 (c)), the slot separates the blade into two parts. The front part is analogous to a "mini blade". The mini blade has a small corner separation with span wise vortex and concentrated shedding vortex as the slot jet has very slight impact on the flow field before its outlet. At the back part, the jet flow accelerates separation fluids with a similar effect of the external jet actuators. The jet flow decreases the size of the passage vortex and separates it off the suction surface. The trailing edge span wise vortex and separation vortex become smaller as the separated airflow is speeded up. The corner vortex is completely eliminated by the jet flow.

In the synthetic configuration (Fig.15 (d)), VG vortex eliminates the span wise vortex and concentrated shedding vortex in front passage. The separation vortex of the "mini blade" is also suppressed and minified by the VG. The slot jet reattaches separation airflow to the suction surface and eliminates vortices in it. The VG and the slot decrease the passage vortex and trailing edge span wise vortex at the same time, and they are all separated away from the suction surface and then minified in size. The vortices structure and separation behaviors in this configuration are well improved by the cooperation of the VG and the slot.

In summary, the synthetic approach is more powerful due to the cooperation of the VG and the slot. The VG suppresses the end wall cross flow and prevents the passage vortex from merging with the corner separation. In this way, it delays separation production and weakens vortices initiated from the end wall. The slot jet flow speed up the separation fluids and reattaches them to the suction surface, and then reduces the vortices behind the slot outlet. As a result, the control impacts on the separation and vortices cover the whole passage.

7. CONCLUSIONS

This paper introduces a synthetic flow control approach and uses it in a high load compressor cascade. Numerical investigations are conducted to study the cascade flow behaviors, the performance improvements and the flow control mechanisms.

(1) The synthetic approach achieves better flow control effects due to the combination. The reason is that the VG reduces the end wall initiated separation in the front of cascade passage while slot reduces the trailing edge separation in the passage back. The VG

vortex suppresses the end wall cross flow and prevents the production of corner separation. The slot speed up the separation fluids and reattaches them to the suction surface, and then reduces the trailing edge separation.

(2) The cascade performance achieves considerable improvements in the VG, the slot, and the synthetic configurations. Averaged in all the operating conditions, the loss decreases 11.03%, 2.92%, and 13.75% respectively; the static pressure rise improves 4.05%, 1.46%, and 4.88% respectively; the flow turning angle improves 0.09%, 0.95%, and 1.91% respectively. The synthetic approach acquires the largest improvements in which the performance parameters are almost the superposition of the two individual ones.

(3) In the synthetic configuration, the VG reverses part of the cross flow which eliminates the span wise vortex and weakens the concentrated shedding vortex. The VG vortex also suppresses the development of the passage vortex by deflecting it. The slot jet blow away vortices behind slot outlet due to the acceleration. VG and slot jet suppress the passage vortex and the trailing edge span wise vortex at the same time. As a result, the control impacts on the vortices cover the whole passage.

In sum, the synthetic approach suppress the production of the end wall secondary flow and the trailing edge separation, forming a more powerful and effective synthetic flow control approach. In the future, experiment measurements will be conducted to verify the synthetic design, and more numerical studies will be conducted to improve the details of the evolution in terms of the separation and the vortex in this study. The possible engineering utilizations in the compressors will also be discussed.

REFERENCES

Akcayoz, E., H. D. Vo and A. Mahallati (2015). Controlling Corner Stall Separation with Plasma Actuators in a Compressor Cascade, *ASME GT2015-43404*.

Chima, R. V. (2002). Computational Modeling of Vortex Generators for Turbo Machinery, ASME GT2002-30677.

Gbadebo, S. A., N. A. Cumpsty and T. P. Hynes (2005). Three-dimensional Separations in Axial Compressors, *Journal of Turbomachinery*, 127(2), 331-339.

Govardhan, M., A. Rajender and J. P. Umang (2006). Effect of Streamwise Fences on Secondary Flows and Losses in a Two-Dimensional Tur-

bine Rotor Cascade, *Journal of Thermal Science* 15(4), 296–305

Guo, S., H. Lu, F. Chen and J. Wu (2013). Vortex Control and Aerodynamic Performance Improvement of a Highly Loaded Compressor Cascade via Inlet Boundary Layer Suction. *Experiments in Fluids* 54(7), 1570.

Hecklau, M., O. Wiederhold, V. Zander, R. King, W. Nitsche, M. Swoboda and A. Huppertz (2013). Active Separation Control with Pulsed Jets in a Critically Loaded Compressor Cascade, *AIAA Journal* 49(8), 1729-1739.

Hergt, A., R. Meyer and K. Engel (2006). Experimental Investigation of Flow Control in Compressor Cascades, *ASME GT2006-90415*.

Hergt, A., R. Meyer and K. Engel (2013). Effects of Vortex Generator Application on the Performance of a Compressor Cascade, *Journal of Turbomachinary* 135(2), 021026.

Hu, J., R. Wang, R. Li, C. He and Q. Li (2017). Experimental Investigation on Separation Control by Slot Jet in Highly Loaded Compressor Cascade, *Proc IMechE Part G: J Aerospace Engineering*, Online Publish.

Hu, J., R. Wang, P. Wu and C. He (2016). Separation Control by Slot Jet in a Critically-Loaded Compressor Cascade, *International Journal of Turbo & Jet Engines*, Online Publish.

Kang S. (1993). Investigation of the Three Dimensional Flow within a Compressor Cascade with and without Tip Clearance, Ph.D. Thesis, Dept. of Fluid Mechanics, Vrije Universiteit Brussel I-1-V-44.

Liu, Y., H. Yan and L. Lu (2016). Numerical Study of the Effect of Secondary Vortex on Three-Dimensional Corner Separation in a Compressor Cascade, *International Journal of Turbo and Jet-Engines* 33(1), 9-18.

Pesteil, A., D. Cellier, O. Domercq, V. Perrot and J. C. Boniface (2010). CREATE: Advanced CFD for HPC Performance Improvement, *ASME GT2010-68844*.

Ramzi, M. and G. Abderrahmane (2013). Passive Control via Slotted Blading in a Compressor Cascade at Stall Condition, *Journal of Applied Fluid Mechanics* 6(4), 571-580.

Varpe, M. K. and A. M. Pradeep (2015). Benefits of Nonaxisymmetric Endwall Contouring in a Compressor Cascade with a Tip Clearance, *Journal of Fluids Engineering* 137(5), 051101

Wu, P., R. Wang, F. Guo, J. Hu and K. Li (2016). Mechanism Analysis of Effects of Vortex Generator on High-Load Compressor Cascade, *Journal of Propulsion Technology* 37(1), 49-56.

Wu, P., R. Wang, J. Hu and F. Guo (2014). Influence of the Location of the Slot at the Outlet on the Performance of a Highly-Loaded Diffusion Cascade, *Journal of Engineering for Thermal Energy and Power* 29(4), 121-126.

Wu, P., R. Wang, K. Luo and F. Guo (2013). Effect of Slotted Blade on Performance of High-Turning Angle Compressor Cascade, *Journal of Aerospace Power* 28(11), 2505-2509.